An ice-cream cone model for coronal mass ejections

X. H. Xue, C. B. Wang, and X. K. Dou

School of Earth and Space Sciences, University of Science and Technology of China, Hefei, Anhui, China

Received 22 July 2004; revised 15 March 2005; accepted 8 April 2005; published 11 August 2005.

[1] In this study, we use an ice-cream cone model to analyze the geometrical and kinematical properties of the coronal mass ejections (CMEs). Assuming that in the early phase CMEs propagate with near-constant speed and angular width, some useful properties of CMEs, namely the radial speed (v), the angular width (α), and the location at the heliosphere, can be obtained considering the geometrical shapes of a CME as an ice-cream cone. This model is improved by (1) using an ice-cream cone to show the near real configuration of a CME, (2) determining the radial speed via fitting the projected speeds calculated from the height-time relation in different azimuthal angles, (3) not only applying to halo CMEs but also applying to nonhalo CMEs.

Citation: Xue, X. H., C. B. Wang, and X. K. Dou (2005), An ice-cream cone model for coronal mass ejections, *J. Geophys. Res.*, *110*, A08103, doi:10.1029/2004JA010698.

1. Introduction

[2] The halo coronal mass ejection (CME), which looked like a bright cloud surrounding the entire Sun and propagating outward from it in all directions, was first reported by *Howard et al.* [1982] and was interpreted as a broad shell or bubble of dense plasma ejected directly toward (or away from) the Earth. Now it is generally accepted that halo CMEs which travel along the Sun-Earth line to the Earth are associated with disturbances of the geomagnetic fields and responsible for many large geomagnetic storms. [e.g., *Gosling et al.*, 1991; *Brueckner et al.*, 1998; *Cane et al.*, 2000; *Gopalswamy et al.*, 2000; *Webb et al.*, 2000; *Wang et al.*, 2002].

[3] Many routine observations of CMEs and the CMEs-associated solar active regions have been established by the Large Angle Spectroscopic Coronagraph (LASCO) and Extreme Ultraviolet Imaging Telescope (EIT) on board the Solar and Heliospheric Observatory (SOHO) [*Brueckner et al.*, 1995; *Delaboudiniere et al.*, 1995], the Soft X-ray Telescope (SXT) on Yohkoh [*Tsuneta et al.*, 1991], etc. The combinations of LASCO and SOHO/EIT observations of the halo CMEs make it possible to determine whether a halo CME is a frontside (toward the Earth) one or a backside (away from the Earth) one [*Plunkett et al.*, 2001]. These routine observations are very helpful for studying the properties of CMEs as well as for space weather forecasting.

[4] Owing to the notable geomagnetic effects of halo CMEs, prediction of the arrival of CME in the vicinity of Earth is critically important in space weather investigations. The determination of the radial propagation speed and acceleration of the frontside halo CME is necessary for more accurate space weather forecasting [*Zhao et al.*, 2002]. *Gopalswamy et al.* [2000] and *Gopalswamy* [2002] developed and improved an empirical model to predict the arrival time of CMEs at 1 AU based on the interplanetary CMEs detected by Wind spacecraft and their corresponding CMEs remote-sensed by SOHO. This increased solar wind speed may be inferred more accurately using this empirical moldel, if the geometrical and kinematical properties of halo CMEs (e.g., the angular width and central position angle of CME, the initial speed of CME) can be determined [*Michalek et al.*, 2004]. However, the angular width and the initial speed of CME obtained directly from the measurement of the observation of LASCO are only the projected angle and speed on the sky plane. They can not be deemed as the real parameters of CME unless the CME is a broadside one, whose latitudinal span of their bright feature in the sky plane being less than 120° so that the angular width and the central position angle can be directly measured based on their latitudinal span [*Zhao et al.*, 2002].

[5] The projection of many broadside CMEs on the sky plane observed by LASCO coronagraph looks like a cone shape, which can maintain this shape and propagation almost radially in the view fields of LASCO/C2 and LASCO/C3. At the same time, the angular width of many broadside CMEs remains constant during their expansion outward [*Webb et al.*, 1997]. These facts indicate that the shell of mass is nearly symmetric about the central position of CMEs. Some authors suggested that the geometrical properties of CMEs may be described by a cone model [*Howard et al.*, 1982; *Fisher and Munro*, 1984; *Leblanc et al.*, 2001; *Zhao et al.*, 2002; *Michalek and Gopalswamy*, 2003; *Xie et al.*, 2004].

[6] *Fisher and Munro* [1984] have proposed a so-called ice-cream cone model to depict the mass and other physical properties used in the specification of the coronal transient model, but in practice this model is suitable only for the broadside CMEs, whose footpoints are located in the limb of the Sun. *Leblanc et al.* [2001] have converted the measured CME progressions in the sky plane into the progressions in the radial direction for the first time, in the light of a new technique which is based on an ice-cream cone like model. However, in their model, the angular width

0148-0227/05/2004JA010698$09.00

of the CME is estimated to a statistical value, and it cannot reflect the characteristics of an individual CME. Recently, *Zhao et al.* [2002] has developed a cone model to estimate the geometrical and kinematical properties of the three-dimensional halo CMEs, using coordinate conversion between the cone system and the heliographic system, and adjusting three free parameters iteratively to best match the LASCO observations. To avoid the ambiguity introduced by visual fitting and computational time-consumption of Zhao's model, *Xie et al.* [2004] has presented an innovative analytical method to determine the relation of cone CME angular width and orientation to its elliptical sky-plane projection and the relation of CME actual radial speed to projection speeds at different position angles. *Michalek and Gopalswamy* [2003] has also given a simple cone model by measurements of the sky plane speeds and the times of the first appearance of the full halo CMEs above opposite limbs. Using the model, *Michalek et al.* [2004] have studied the arrival time of the halo CMEs in the vicinity of the Earth. The accuracy of prediction is improved.

[7] In this paper, we will present an ice-cream cone model to estimate the parameters (velocity, angle width, and source location) of the CMEs. This model can exhibit the near real geometrical characteristics of CME from its projected speeds measured at different directions in the sky plane.

[8] The structure of the paper is outlined as follows. In section 2, the model is described in detail. Section 3 examines the validity of this ice-cream cone model. Finally, we present discussion and conclusions in section 4.

2. Ice-Cream Cone Model

[9] Assuming that a CME is isotropic and is emitted from a point, one can image that the front edge of the CME should form a sphere-like shape. Thus we consider that (1) the shape of CMEs is a symmetrical ice-cream cone, combining a cone with a sphere. The apex of the cone and the center of the sphere are all located at the center of the Sun. Figure 1 shows a sketch map of the ice-cream cone model. (2) The propagations of CMEs are nearly radial. (3) The velocities and angular widths of the CMEs remain constant. Then, the projected front edge of CMEs in the sky plane is determined by the projection of the sphere cross section of the ice-cream cone. The widths, velocities, and the source location of CMEs can be estimated through the observation of LASCO/C2 and LASCO/C3.

[10] First, we introduce a heliocentric coordinate system (x_h, y_h, z_h), where the x_h axis points to the Earth and (y_h, z_h) defines the sky plane. Assuming that we have known the orientation of the ice-cream cone (θ_0, ϕ_0) in heliocentric coordinate, where θ_0 and ϕ_0 are the colatitude and longitude measured from the central meridian, we can establish the cone coordinate system (x_c, y_c, z_c) through the rotation of coordinate (x_h, y_h, z_h) as shown in Figure 1. Letting (x_h, y_h) plane rotate around the z_h through the angle ϕ_0, we get a coordinate (x', y', z'). Then the cone coordinate system (x_c, y_c, z_c) is established by making another rotation of (x', z') around y' through the angle θ_0. Note that in cone coordinate system, z_c parallel to the ice-cream cone axes and its orientation describes the propagation direction of CME.

[11] The transform between the heliocentric coordinate system (x_h, y_h, z_h) and the cone coordinate system (x_c, y_c, z_c)

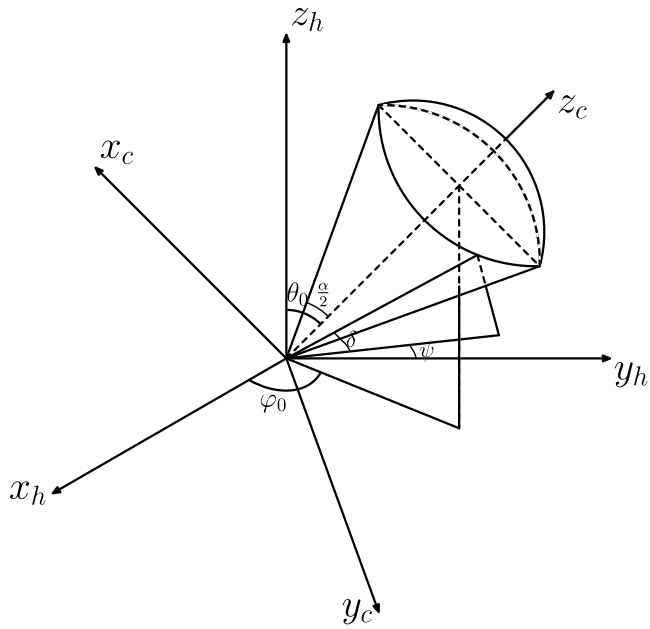

Figure 1. A sketch map of the ice-cream cone model and the relationship between the heliocentric coordinate system and the cone coordinate system.

can be carried out as

$$\begin{pmatrix} x_h \\ y_h \\ z_h \end{pmatrix} = M \begin{pmatrix} x_c \\ y_c \\ z_c \end{pmatrix} \tag{1}$$

or

$$\begin{pmatrix} x_c \\ y_c \\ z_c \end{pmatrix} = M^{-1} \begin{pmatrix} x_h \\ y_h \\ z_h \end{pmatrix}, \tag{2}$$

where

$$M = \begin{pmatrix} \cos\theta_0 \cos\phi_0 & -\sin\phi_0 & \cos\phi_0 \sin\theta_0 \\ \cos\theta_0 \sin\phi_0 & \cos\phi_0 & \sin\phi_0 \sin\theta_0 \\ -\sin\theta_0 & 0 & \cos\theta_0 \end{pmatrix},$$

$$M^{-1} = \begin{pmatrix} \cos\theta_0 \cos\phi_0 & \cos\theta_0 \sin\phi_0 & -\sin\theta_0 \\ -\sin\phi_0 & \cos\phi_0 & 0 \\ \cos\phi_0 \sin\theta_0 & \sin\phi_0 \sin\theta_0 & \cos\theta_0 \end{pmatrix}.$$

In the cone coordinate system, the cone equation is easy to be described as

$$\cos\theta_c \geq \cos\frac{\alpha}{2}, \tag{3}$$

Table 1. Ice-Cream Cone Model for Possible Cases of CMEs

Types of CME		Projection Speed v_p
Disk-center-covered CMEs	No intersection with sky plane	$v_p = v\cos\delta = v\left\lvert\frac{A\cos\frac{\alpha}{2} \pm C\sqrt{A^2+C^2-\cos^2\frac{\alpha}{2}}}{A^2+C^2}\right\rvert$ $\psi \in [0, 2\pi]$
$(\cos\frac{\alpha}{2} \le \sin\theta_0\cos\phi_0)$	$(\sin\frac{\alpha}{2} < \sin\theta_0\cos\phi_0)$	
	Intersection with sky plane	$\begin{cases} v_p = v\cos\delta = v\left\lvert\frac{A\cos\frac{\alpha}{2} \pm C\sqrt{A^2+C^2-\cos^2\frac{\alpha}{2}}}{A^2+C^2}\right\rvert & \psi \notin [\psi_1, \psi_2] \\ v_p = v & \psi \in [\psi_1, \psi_2]. \end{cases}$
	$(\sin\frac{\alpha}{2} \ge \sin\theta_0\cos\phi_0)$	
Non-disk-center-covered CMEs	No intersection with sky plane	$v_p = v\cos\delta = v\left\lvert\frac{A\cos\frac{\alpha}{2} \pm C\sqrt{A^2+C^2-\cos^2\frac{\alpha}{2}}}{A^2+C^2}\right\rvert$ $\psi \in [\psi_L, \psi_R]$
$(\cos\frac{\alpha}{2} > \sin\theta_0\cos\phi_0)$	$(\sin\frac{\alpha}{2} < \sin\theta_0\cos\phi_0)$	
	Intersection with sky plane	$\begin{cases} v_p = v\cos\delta = v\left\lvert\frac{A\cos\frac{\alpha}{2} \pm C\sqrt{A^2+C^2-\cos^2\frac{\alpha}{2}}}{A^2+C^2}\right\rvert & \psi \in [\psi_L, \psi_R] \cap \overline{[\psi_1, \psi_2]} \\ v_p = v & \psi \in [\psi_1, \psi_2]. \end{cases}$
	$(\sin\frac{\alpha}{2} \ge \sin\theta_0\cos\phi_0)$	

where α is the angular width of the cone and θ_c is the angle measured from the z_c axis. Using equation (2), we can get the cone equation in heliocentric coordinate system

$$1 \ge \frac{x_h\cos\phi_0\sin\theta_0 + y_h\sin\phi_0\sin\theta_0 + z_h\cos\theta_0}{\sqrt{x_h^2+y_h^2+z_h^2}} \ge \cos\frac{\alpha}{2}. \quad (4)$$

[12] The ice-cream cone shell is defined as the overlap area between the cone and a sphere with radius r_c, which should satisfy

$$\begin{cases} 1 \ge \dfrac{x_h\cos\phi_0\sin\theta_0 + y_h\sin\phi_0\sin\theta_0 + z_h\cos\theta_0}{r_c} \ge \cos\dfrac{\alpha}{2}, \\ x_h^2 + y_h^2 + z_h^2 = r_c^2 \end{cases} \quad (5)$$

where r_c is the heliocentric distance of the CME's front side.

[13] When the cone has no intersection with the sky plane, it can be demonstrated that the projected contour of the sphere cross section in the ice-cream cone model is as same as the one of the circle cross section in the cone model. From the equation (5), one can find that the angle δ between an arbitrary generatrix on the cone surface and the plane of sky (OY_hZ_h plane) satisfies

$$\sin\delta = \frac{\cos\frac{\alpha}{2}\cos\phi_0\sin\theta_0 \pm A\sqrt{\cos^2\phi_0\sin^2\theta_0 + A^2 - \cos^2\frac{\alpha}{2}}}{\cos^2\phi_0\sin^2\theta_0 + A^2}, \quad (6)$$

and A is defined by

$$A = \cos\psi\sin\phi_0\sin\theta_0 + \sin\psi\cos\theta_0, \quad (7)$$

where ψ is the azimuthal angle of a cone generatrix's projection in OY_hZ_h plane, measured from y_h axis.

[14] One can find that equation (6) has real root for any given $\psi \in [0, 2\pi]$, if $\cos\frac{\alpha}{2} \le \cos\phi_0\sin\theta_0$. The implication is that the origin of the coordinate OY_hZ_h is encircled by the projection of the ice-cream cone on the sky plane. This CME is a disk-center-covered CME, which includes the cases of the full halo CME and the disk-center-covered partial halo CME (that satisfies the condition $\cos\frac{\alpha}{2} \le \cos\phi_0\sin\theta_0$ but does not develop as a full halo in the LASCO view field).

[15] If $\cos\frac{\alpha}{2} > \cos\phi_0\sin\theta_0$, equation (6) has real roots only for $\psi_L \le \psi \le \psi_R$. The origin of the coordinate OY_hZ_h is out of the projected region of the ice-cream cone. This CME is non-disk-center-covered CME. Here, $\psi_L = \psi_0 + \psi_-$, $\psi_R = \psi_0 + \psi_+$, ψ_0 and $\psi_\pm$ are the azimuthal angle of the projected ice-cream-cone axis on sky plane and the half-width of the projected angle of the ice-cream cone on the sky plane, respectively. One can get

$$\tan\psi_0 = \frac{\cos\theta_0}{\sin\theta_0\sin\phi_0} \quad (8)$$

and

$$\cos\psi_\pm = \pm\frac{\sqrt{\cos^2\frac{\alpha}{2} - \sin^2\theta_0\cos^2\phi_0}}{\sqrt{\sin^2\theta_0\sin^2\phi_0 + \cos^2\theta_0}}. \quad (9)$$

[16] In our model, the criteria between a disk-center-covered CME and a non-disk-center-covered CME is whether the projected angular width (PAW) of the ice-cream cone on the sky plane is greater than 180° or not. The relationship of $\cos\frac{\alpha}{2} = \sin\theta_0\cos\phi_0$ specifies the boundary between this two types of CME in the ice-cream cone model. This is different from the angle of 120°, which is often used in LASCO observation to distinguish between a halo CME and a nonhalo CME. For a disk-center-covered CME, although the origin of the coordinate OY_hZ_h is encircled by the projected region of the ice-cream cone, whether the projection of the ice-cream cone in the view of LASCO observation is a full halo or not, depending on the orientation, angle width, and the radial distance of the ice-cream cone because the projected shape of

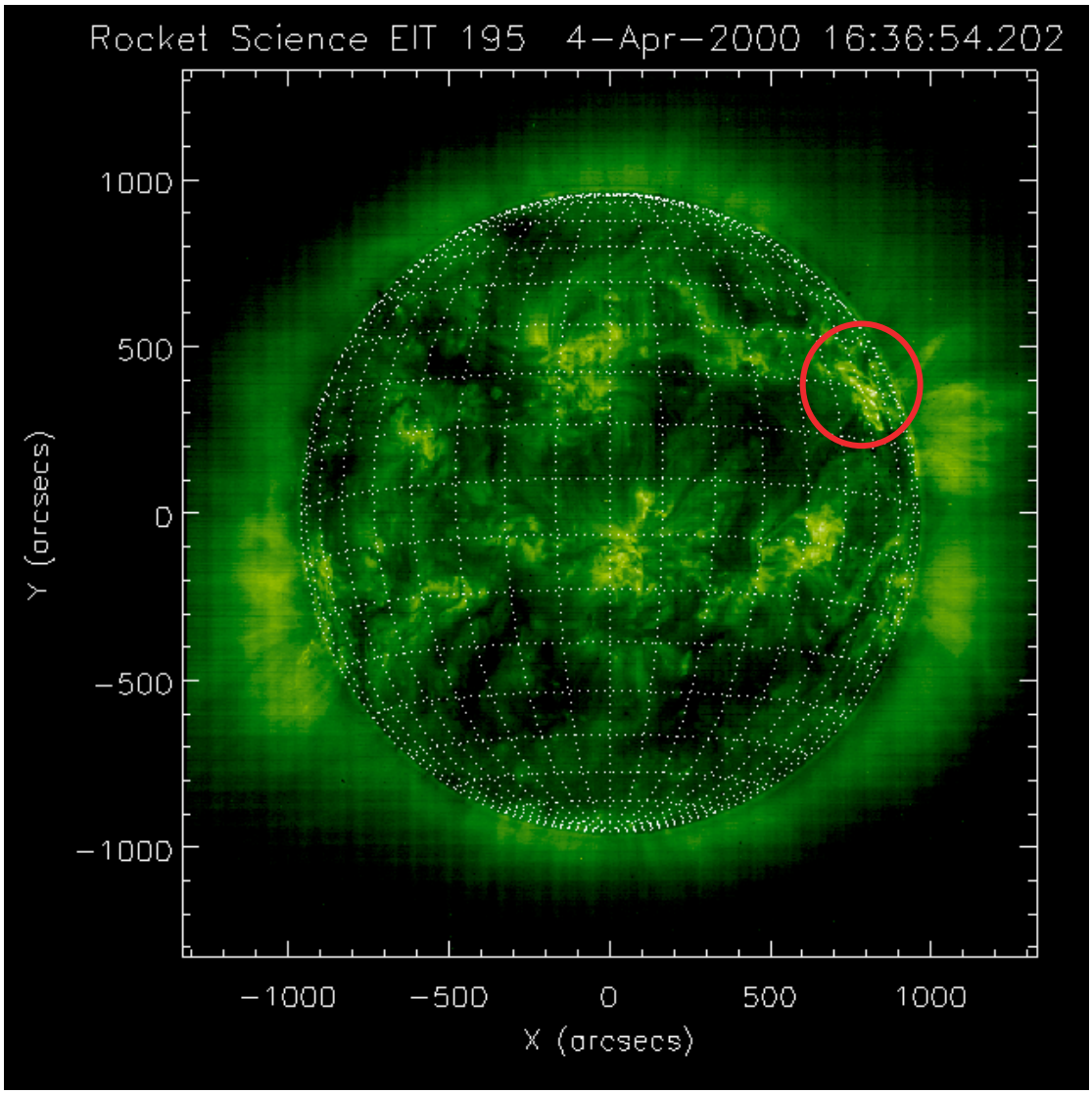

Figure 2. The SOHO/EIT observation of the event on 4 April 2000, and there was a C9.7 flare in active region 8933 marked by the circle associated with the CME at N19W56 begun at 1512 UT.

the ice-cream cone on the sky plane changing as the orientation, angle width, and the radial distance change [see *Zhao et al.*, 2002, Figures 1 and 2].

[17] If the ice-cream cone intersects with the sky plane OY_hZ_h, the speed of the projection in the intersectant region will be equal to the radial speed of CME in the intersectant region. Assuming that the intersectant area is $\psi_1 \le \psi \le \psi_2$, let $\sin\delta = 0$ in equation (6), one can get the following equation

$$\begin{cases} \cos\psi_{1,2}\sin\phi_0\sin\theta_0 + \sin\psi_{1,2}\cos\theta_0 = \cos\dfrac{\alpha}{2} \\ \sin\dfrac{\alpha}{2} \ge \sin\theta_0\cos\phi_0 \end{cases} \tag{10}$$

[18] Now we can establish the relationship between the projected speed v_p in the sky plane and bulk speed v, according to the above discussion. The projections of the CMEs on the sky plane can be divided into four possible cases, the disk-center-covered CMEs with or without sky-plane intersection and the non-disk-center-covered CMEs with or without sky-plane intersection, as shown in Table 1. Note that $C = \sin\theta_0\cos\phi_0$ for all the cases discussed.

[19] The other necessary parameters γ (the angle between the axis of the cone and the sky plane) can be obtained from the following equation:

$$\sin\gamma = \sin\theta_0\cos\phi_0. \tag{11}$$

The position angle (PA) defined counter clockwise in degrees from solar north in the LASCO imaging plane can be obtained from equation (8).

3. Parameter Determination of the Ice-Cream Cone Model

3.1. Application of the Ice-Cream Cone Model to a Full Halo CME on 4 April 2000

[20] From the equations in Table 1, there are four parameters needed to be determined, namely, the radial speed of

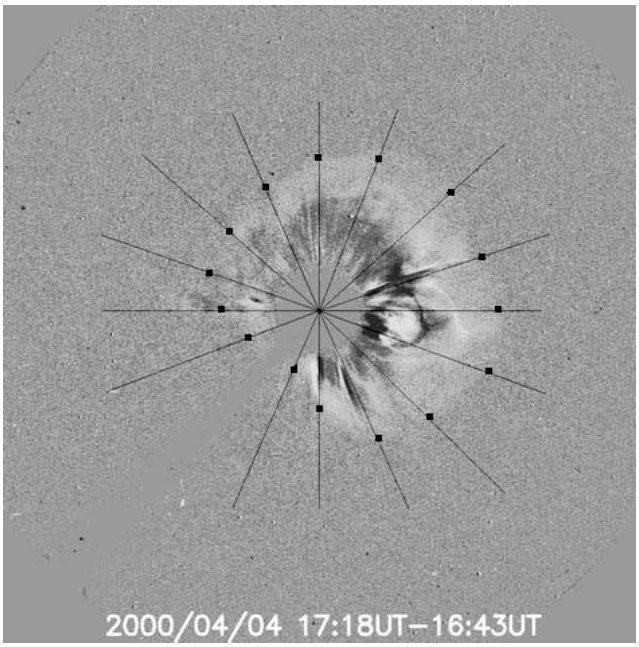

Figure 3. The running different image of the propagation of the CME (1718–1643 UT) on 4 April 2000. The radial lines show the given directions and the solid squares show the measured front edge of the CME.

the CME (v), the angular width of the CME (α), and the location of the CME (θ_0, ϕ_0). In following part, we will illuminate how to determine these parameters of a full halo CME using a case observed on 4 April 2000 (the same case as used by *Xie et al.* [2004]).

Table 2. Measured Projection Speeds of the CME on 4 April 2000 in Different Directions

Angle, deg	Speed, km/s
12.6°	1074.6
25.7°	1114.3
36.3°	1242.4
43.9°	1109.1
55.3°	1125.2
67.3°	1103.2
78.6°	1101.2
91.2°	993.3
99.7°	977.3
115.2°	828.0
133.0°	754.3
152.2°	687.9
167.2°	612.4
183.8°	514.3
201.2°	508.2
215.9°	506.0
238.6°	545.9
254.6°	593.5
270.2°	687.9
282.0°	788.9
294.2°	923.6
307.4°	994.1
319.3°	1091.7
330.3°	1130.9
343.3°	1162.6
357.8°	1124.2

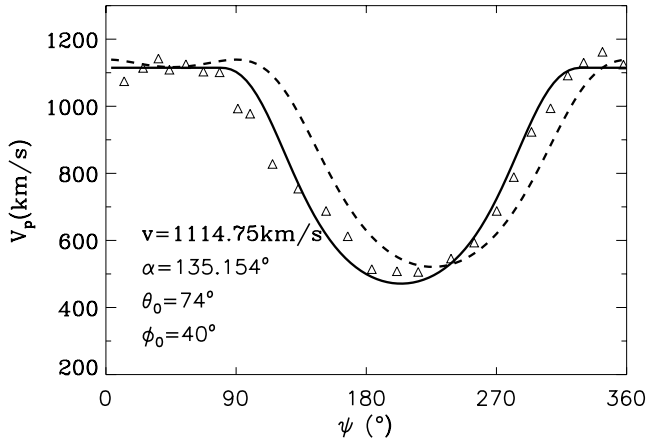

Figure 4. The distribution of the projection speed on the azimuthal angle ψ in the sky plane for the 4 April 2000 CME. The triangles show the measured data. The solid curve is the fitting result using the ice-cream cone model, and the dashed curve is obtained from Xie et al.'s work.

[21] To determine these parameters mentioned above, three steps are considered: (1) Restricting the possible source region from the SOHO/EIT observations; (2) Measuring the height-time relations to obtain the projected speeds on different azimuthal angles; (3) In the possible source region estimated in step 1, using the least-squares fit method to decide the best fit parameters.

[22] First, the erupted point (θ_0, ϕ_0) the CME is restricted to a relatively small region based on the SOHO/EIT observations. Figure 2 shows the SOHO/EIT observation of the event on 4 April 2000. There was a C9.7 flare in active region 8933 marked by the circle associated with the CME at N19W56 begun at 1512 UT. Owing to the fact that CME-associated flares or active regions are often located near one leg of CMEs, rather than near the center [*Harrison*, 1986; *Plunkett et al.*, 2001], we can confine the location of the apex of the ice-cream cone (θ_0, ϕ_0) to a relatively reasonable region from the EIT observation. In this case, we confined θ_0 and ϕ_0 in a $36° \times 36°$ region centered on the point N19W56. That is, the region encircled by the heliacal latitude [N01, N37] and the heliacal longitude [W38, W74].

[23] Second, measuring the projected speeds of the CME in different directions via the height-time relations. Using the Solar Software SSW (http://www.lmsal.com/solarsoft/), we can get a series of the running different images of the LASCO C2 and C3 observations. Figure 3 shows a running different image of LASCO/C3 at 1718 UT of the event 4 April 2000. We establish some radials emitted from one origin point to label the azimuthal angles (i.e., the angle ψ in Table 1) on the sky plane, on which the height-time relations will be obtained. To ensure that the azimuthal angles of different images are the same, the centers of LASCO planes in different images are all located on this origin point (see Figure 3).

[24] We mark the front edges of the CME on different azimuthal angles at a given time (see the points marked in the sketch Figure 3). Through recording the propagations of the marked points at different time, one can get

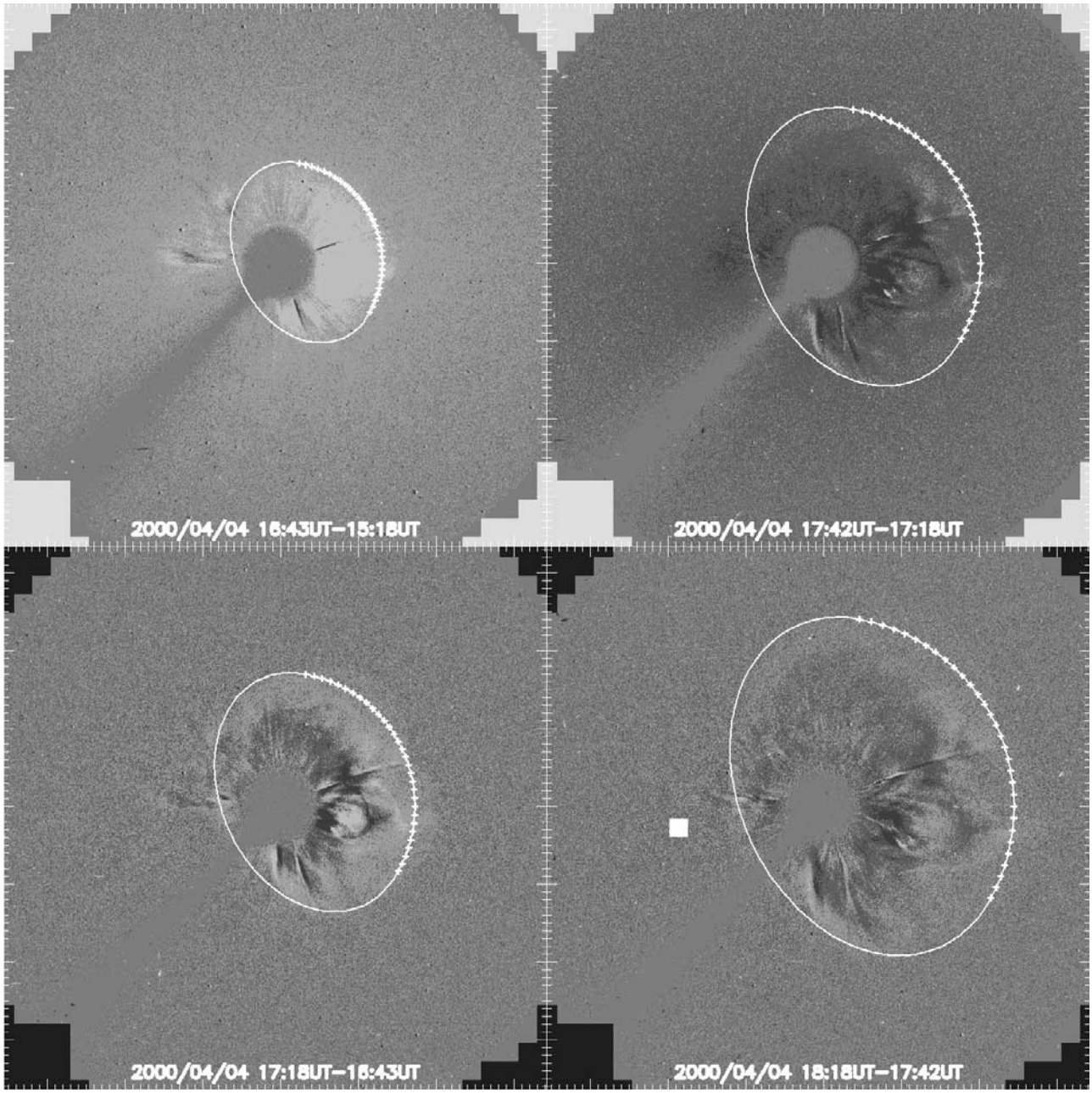

Figure 5. Comparison of the modeled halos (white circles) and the LASCO difference images from the 4 April 2000 CME. The intersection region of the model with the sky plane is denoted by the crosses.

the height-time relations on every labelled azimuthal angle. The observed projected speeds ($v_{p,obs}$) of the CME on this azimuthal angle can be obtained by linear fitting the height-time relations. Table 2 shows the linear fitting $v_{p,obs}$ versus the azimuthal angles for the CME on 4 April 2000.

[25] Finally, the optimal parameters v, α, and proper (θ_0, ϕ_0) can be determined by the least-squares fit of the calculated projected speeds ($v_{p,cal}$) (obtained from the equations in Table 1) with the measured projection speeds ($v_{p,obs}$) on different azimuthal angles. For the case on 4 April 2000, we obtain v = 1114.75 km/s, α = 135.15°, θ_0 = 74°, ϕ_0 = 40°, γ = 47.4°, and PA = 294.0° with a least-squares deviation σ_v = 77.2 km/s. At the same time, it has been found that this full halo CME had an intersection with the sky plane in the range of $\psi \in [328.4°,79.7°]$. Figure 4 shows the plot of the calculated projected speeds using the above optimal parameters versus the measured projection speeds. The triangles indicate the measured speeds. The solid line is the curve of the calculated projection speeds on the sky plane. The beelines at the both sides of the curve indicate that the ice-cream cone has intersected with the sky plane at the azimuths in the region [328.4°,79.7°] and the projected speeds should reflect the real radial speed of the CME.

Table 3. Comparison of the Cone Parameters for the CME on 4 April 2000 Derived From Three Methods

	V, km/s	α	θ_0	ϕ_0	γ	*PA*
Ours	1114.75	135.15°	74°	40°	47.4°	294.0°
Xie et al.	1139.1	128.6°	64.3°	27.7°	53.3°	316.1°
Michalek et al.	1645	151°	–	–	37°	304°

[26] Having these geometrical parameters of the ice-cream cone, we can reproduce the propagation of the CME with time from the height-time relation. For example, we can obtain the real radial distance r of the ice-cream cone shell at time 1643 UT by fitting the projected distances (that are recorded by the squares in Figure 3) at that time using the parameters of α, θ_0, and ϕ_0. Then, the reproduced cross section of the ice-cream cone on the sky plane can be plotted (see the white circle on the first picture of Figure 5). On the basis of the r at 1643 UT, one can easy decide the following cross section of the ice-cream cone on the sky plane versus time series. Figure 5 shows the projection of the modeled full halo CME (white circles) propagated with time, which are superposed on the running different images observed by LASCO/C3, and the intersected region are denoted by the crosses.

[27] This event has also been discussed by *Michalek and Gopalswamy* [2003] and *Xie et al.* [2004]. In work by Michalek and Gopalswamy, the width, speed, and source location of the halo CME were obtained by measuring the sky-plane speeds of the first appearance of the halo CME above opposite limbs on LASCO observations. Xie et al. used an ellipse in the sky plane to fit the observations of LASCO and obtain the cone parameters. Their results are also listed in Table 3. A discussion and a comparison on the results obtained from these three models will be given in the following section.

3.2. Application of the Ice-Cream Cone Model to a Broadside CME on 26 October 2003

[28] There is a little difference between application of the ice-cream cone model to a disk-center-covered CME and to a non-disk-center-covered CME. From the LASCO observations, the projected angular width (PAW) ($\psi_L \leq \psi \leq \psi_R$) on sky plane can be measured so that the azimuthal angle ψ_0 of the projected ice-cream-cone axis and the half-width of the projected angle of a CME ($\psi_\pm$) can be easily determined from observations. Comparing these measured values with the calculated ones from equations (8) and (9), we can constrain the selects of θ_0, ϕ_0 and α in step 3.

[29] For a non-disk-center-covered CME on 26 October 2003, we got the observational $\psi_0 = 5.0°$ and $\psi_\pm = \pm 78.96°$. Thus the geometrical parameters are $\theta_0 = 86°$, $\phi_0 = 57°$, $\alpha = 110°$, and the kinematic parameter of this CME is $v = 1589.0$ km/s. Comparing with the observational erupted location N05W43 (determined from the EIT observation), one can find that the location parameters $\theta = 86°$ and $\phi = 57°$, that is, N04W57, obtained from this method, are reasonable on a certain extent.

[30] The distribution of the projection speeds are shown in Figure 6, where the solid curve shows the least-squares fitting result and the triangles show the measured data. This CME also had an intersection with the sky plane in the range of $\psi \in [319.1°, 52.9°]$. The angle between the axis of the ice-cream cone and the sky plane γ is equal to 32.9°. Figure 7 shows the modeled non-disk-center-covered CME (white circles) propagated with time versus the real running different images observed by LASCO C3 from the 26 October 2003 event.

4. Summary and Discussion

[31] We have fitted 40 frontside halo CMEs (with observational PAW larger than 120°) during 2000–2002 using the ice-cream cone model. The list of these events is shown in Table 4, in which we select all the events from 2000–2002 in the work of *Wang et al.* [2004, Table 1] (in their work, they use samples listed by *Cane and Richardson* [2003] and exclude the ambiguous events and the events resulted from multiple CMEs marked with "i" and "j" in Cane and Richardson's work to make the facts more clear). In Table 4, columns 1–5 give the observational date, time, location, the linear fit speed, and the average transit speed of the CME, respectively. Columns 6–9 give the calculated parameters of the ice-cream cone mode. The last column shows the type of CME defined by the predicted observation angle width (POAW) of the CME in the view field of LASCO/C3 using the ice-cream cone model, namely, the full halo CME ($POAW = 360°$), the disk-center-covered partial halo CME ($180° < POAW < 360°$), and the non-disk-center-covered CME ($POAW < 180°$). Please note that full halo CME and the disk-center-covered

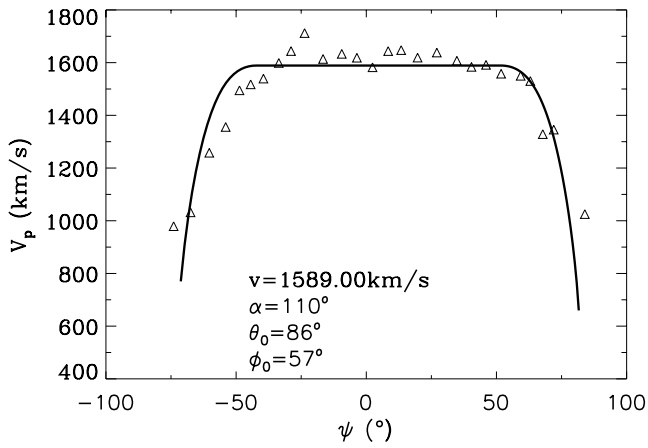

Figure 6. The distribution of the projection speed on the azimuthal angle ψ in the sky plane for the 28 October 2003 CME. The triangles show the measured data. The solid curve is the fitting result using the ice-cream cone model.

Table 4. List of the Geometrical and Kinematic Parameters of the Frontside CMEs (>120°) Obtained Through Ice-Cream Cone Model During 2000–2002[a]

CMEs					Ice-Cream Cone				
Date	Time	Location	V_f^b km s^{-1}	V_f^c km s^{-1}	V, km/s	α, deg	Location	Intersection, deg	Char[d]
					2000				
01/18*	1754	S16E04	739	438.6	756.0	148.8	S09E15	(184.9,247.9)	F
02/08	0930	N27E15	1079	530.8	879.0	130.6	N16E15	0	F
02/10	0230	N25E02	944	724.6	920.0	95.0	N16W07	0	F
02/17	2006	S23W15	600	508.1	797.0	99.9	S05W08	0	F
04/04	1632	N19W54	1188	666.7	1114.8	135.2	N16W40	(328.4,79.7)	F
05/10[e]	2006	S26W10	641	603.9	-	-	-	-	-
05/20*	1450	S37W45	348	621.9	417.8	116.0	S40W54	(259.2, 6.7)	N
07/07*	1026	N23W41	453	476.2	560.5	179.1	N21W30	(308.3,126.8)	F
07/11	1327	N18E36	1078	850	1104.5	100.1	N08E26	0	F
07/14*	1054	N17W02	1674	1302.1	1115.0	179.9	N11W13	(310.9,130.7)	F
07/23*	0530	N05E20	613	450.5	551.0	157.5	S04E30	(120.8,255,2)	P
08/09	1630	N20E12	702	688.7	745.7	108.3	N13E08	0	F
09/05	0554	N22E10	473	496.0	785.8	68.0	N37E07	0	N
10/02	2026	S10W01	525	646.0	930.3	66.6	S06W09	0	F
10/09	2350	N02W06	798	520.8	2170.5	36.8	N05W04	0	F
10/25	0826	N20W66(?)	770	493.1	950.8	117.2	N11W26	0	F
11/08*	2306	N09W75	1345	1190.5	1750.3	169.5	N06W50	(284.6,90.9)	F
					2001				
02/28	1450	S17W05	313	490.2	540.7	111.1	S05E05	0	P
03/16*	0350	S08W09	271	490.2	551.0	164.8	S14W17	(250.3,287)	P
03/29*	1026	N15W12	942	636.1	848.3	179.8	N25W14	(332.7,152.4)	F
04/10	0530	S23W09	2411	1028.8	2765.0	54.5	S06W07	0	F
04/11	1331	S22W27	1103	957.9	1268.5	103.1	S19W15	0	F
04/26	1230	N23W02	1006	841.8	950.8	127.1	N22W00	0	F
08/14[f]	1601	N37E17	618	548.2	-	-	-	-	-
09/28	0854	N12E18	846	586.9	1176.3	86.6	S09E05	0	F
09/29*	1154	N14E02	509	578.7	674.0	87.4	N07E10	0	P
10/09	1130	S30E10	973	666.7	950.8	115.0	S23E01	0	F
10/19	1650	N16W30	901	757.6	786.8	144.2	N25W24	(349.4,108.7)	F
10/22[e]	1826	S18E18	618	410.2	-	-	-	-	-
10/25	1526	S18W20	1092	406.5	899.5	122.7	S12W14	0	F
11/04	1635	N06W18	1810	793.7	1719.5	143.9	N11W22	(345.8,69.1)	F
11/22	2330	S17W35	1437	1082.3	2519.0	60.8	N03W11	0	F
					2002				
02/12	1506	N12E38	448	621.9	479.5	75.0	N19E44	0	N
03/15	2306	S07W08	907	534.2	879.0	148.0	S00W17	(340.5,19.5)	F
04/17	0826	S13W12	1218	656.2	1104.5	108.8	S05W24	0	F
05/22*	0326	S15W70	1494	1028.8	1125.0	169.1	S24W50	(246.6,53.1)	F
07/29	1145	S12W16	556	473.5	643.3	109.8	S12W16	0	F
08/16	1230	S10E19	1459	582.8	1401.7	97.9	S15E10	0	F
09/05	1654	N12E27	1657	706.2	2990.5	40.6	S05E15	0	F
09/17	0754	S10W33	960	694.4	1063.5	68.0	S15W29	0	N

[a]Asterisks denote the cases that are not very well fitted.
[b]The linear fit speed of the CME published in CMElist website http://cdaw.gsfc.nasa.gov/CME_list/.
[c]The average transit speed of the CME in the interplanetary medium [*Wang et al.*, 2004].
[d]The type of the CMEs predicted from the ice-cream cone model. F is full halo CME ($POAW = 360°$), P is disk-center-covered partial halo CME ($360° < POAW \leq 180°$), and N is non-disk-center-covered CME ($POAW < 180°$).
[e]The LASCO observations are ambiguous due to the successive CMEs.
[f]Denotes bad LASCO data.

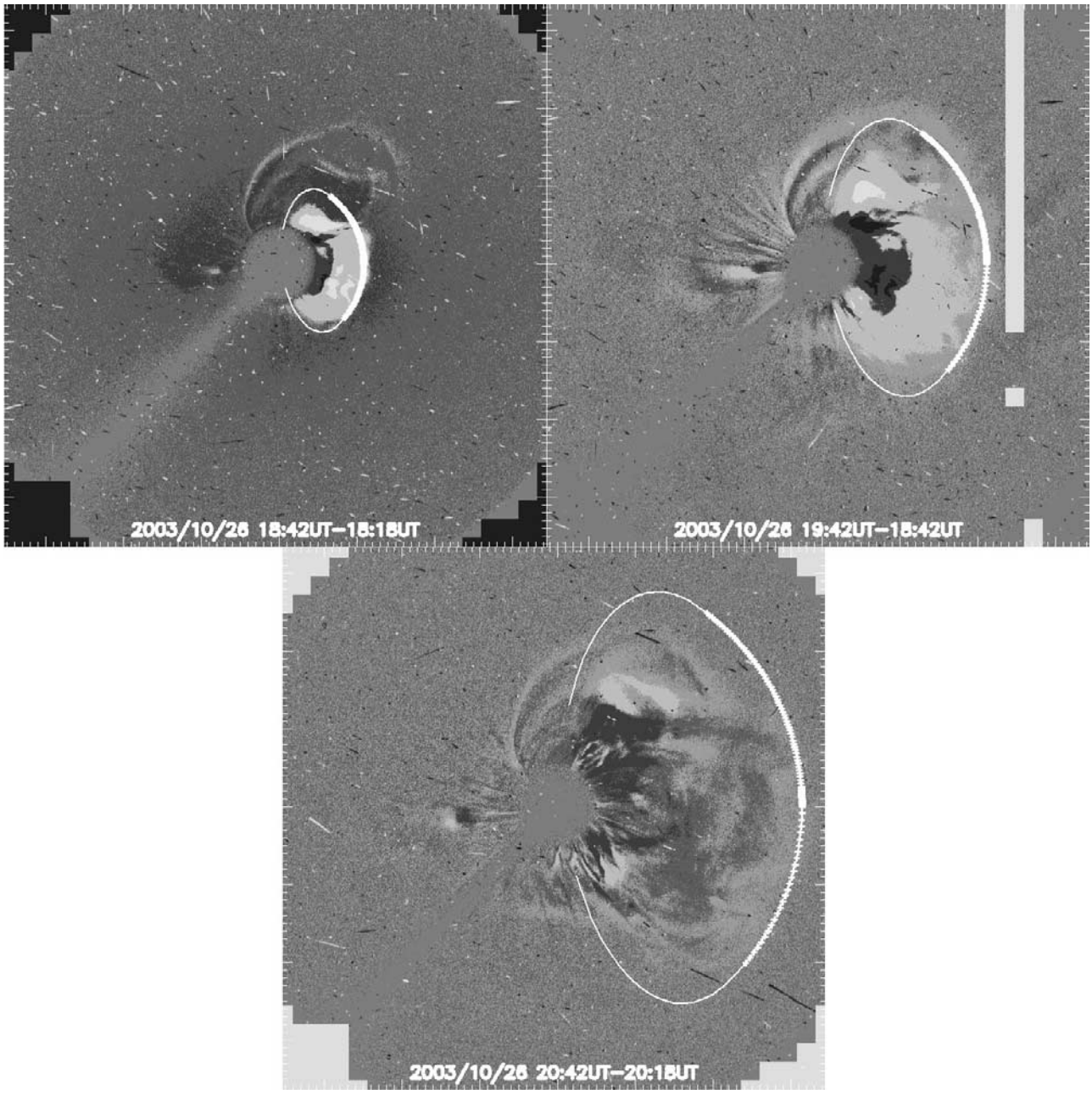

Figure 7. Comparison of the modeled halos (white circles) and the LASCO difference images for the 28 October 2003 CME. The intersection region of the model with the sky plane is denoted by the crosses.

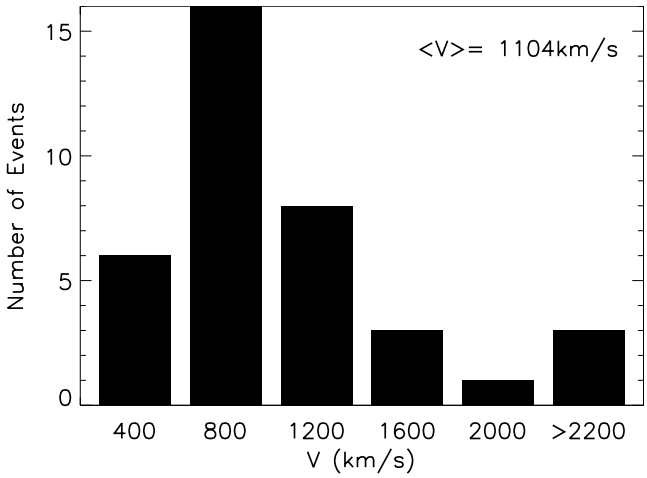

Figure 8. The histogram showing the distribution of V for the halo CMEs listed in Table 4.

partial halo CME here have no distinction in the process of the ice-cream model. They are different only on the LASCO observations because the partial CME just does not develop to a full halo in the view field of LASCO observation, due to the orientation, angle width, and the radial distance of the ice-cream cone [*Zhao et al.*, 2002].

[32] The cases of ambiguous LASCO observations due to successive CMEs erupted or bad LASCO observational data cannot be measured and are marked with e and f, respectively, in Table 4. The cases whose fitting projected speeds curves do not match the measured observational projected speeds data well are marked with stars in Table 4. The possible causes of these unmatched cases are described as following: Some cases, i.e., the CMEs on 14 July 2000 and 29 March 2001, whose angular widths are near 180°, are due to the very symmetrical LASCO observations and with relatively deflected locations from the center of the Sun; some cases have no relatively regular projected contours, i.e., the CMEs on 7 July 2000 and 16 March 2001 or have no very clear observational pictures, i.e., 8 November 2000. The histograms of the speed distribution and the angular width distribution are shown in Figures 8 and 9. The average speed of the CME is 1104 km/s. The average width of the CME is approximately equal to 114° (with the most narrow CME width of 36.8° and the widest one of 179°).

[33] In summary, we use an ice-cream cone model to determine the geometrical and kinematical properties of halo CMEs as well as nonhalo CMEs. Comparing with the previous cone model in the literature, there are some new characteristics in this model.

[34] First, the height-time relationship and the coordinate system transformation are used in this model. From the measurements of height-time relations in different azimuthal angles, one can get the nearly actual distributions of sky-plane observational speeds. It can avoid the ambiguities in finding the point which appears as the first above the occulting disk (that was used in the work of *Michalek and Gopalswamy* [2003]). Moreover, it also give us a way to test whether the parameters of a CME get from the model match the observation well.

[35] Second, this method uses the SOHO/EIT observations to restrict the source locations to a relative small region. It will reduce calculating time and give relatively accurate locations near the active regions. For example, in the case of 4 April 2000, the fitted location is (θ_0, ϕ_0) = (74°, 40°) (that is, N16W40). This location is near to the center the flare active region N19W56, while Xie et al.'s result (θ_0, ϕ_0) = (64.3°, 27.7°) (that is, N26W28) departs more from the flare region. From the Figure 4, one can also find this departure from the observation data.

[36] Third, we also use the ice-cream cone model to fit a nonhalo CME. Halo CMEs and nonhalo CMEs have no essential differences in their geometrical and kinematical properties. The basic methods are the same only with some identifications of observational measurements, namely, identification of the borders of ψ_L, ψ_R in equations in Table 1 from the LASCO observations. Similar work has also been done by *Liu et al.* [2002] using the method developed by *Zhao et al.* [2002].

[37] Finally, the ice-cream cone model is different from previous cone models in the intersectional region between the cone and the sky plane. In this region, the projection is determined by the top coronal of the ice-cream cone. For the event of 4 April 2000, the least-squares deviations calculated by the ice-cream cone model and the cone model are 77.2 km/s and 83.3 km/s, respectively. The difference is not very clear, which is due to the small intersected angle $IA = \alpha/2 - \gamma \approx 20°$ and $\cos IA \approx 0.94$. For the event of 26 October 2003, the least-squares deviations obtained from the ice-cream cone model and the cone model are 66.5 km/s and 132.8 km/s, respectively. Figure 10 shows the projected speed profiles for a given CME with fixed parameters of V = 1000 km/s, α = 120°, θ = 90°, and the longitude ϕ changing from 50° to 80°. One can find that out of the intersectional region the ice-cream cone model and the cone model give the same

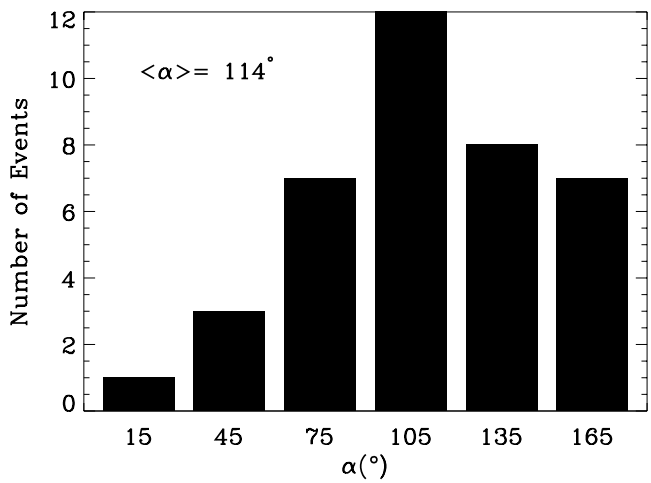

Figure 9. The histogram showing the distribution of α for the halo CMEs listed in Table 4.

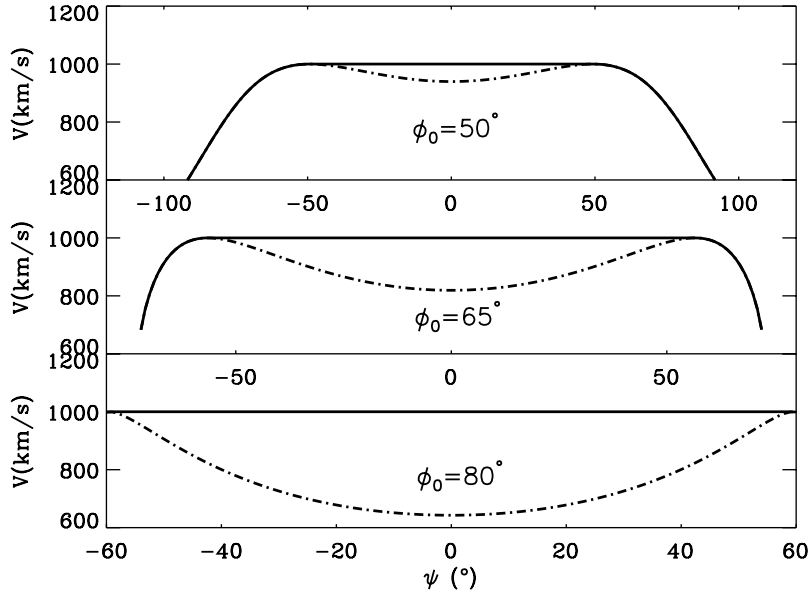

Figure 10. The projection speed profiles on the sky plane for a given CME with V = 1000 km/s, α = 120°, θ = 90°, and ϕ changing from 50° to 80°. The results obtained from the ice-cream cone model and the cone model are shown by the solid line and the dashed line, respectively. The intersection region between the cone and the sky plane is indicated by the horizontal line.

results, but in intersectional region, they give very different results.

[38] Most of the slow CMEs (V < 250 km/s) show acceleration while most of the fast CMEs (V > 900 km/s) show deceleration [*Gopalswamy et al.*, 2000; *Yashiro et al.*, 2004]. We have examined the height-time curve in different azimuths for each case listed in Table 4. In most cases, we found that the height-time plots show nearly linear relations in their measured azimuths with small accelerations (or decelerations). However, the accumulated effect of the small acceleration (or deceleration) will change the initial and final speed of the CME due to the large view field of LASCO. Thus the assumption of constant speed will be not suitable for some cases. This is one of the major error sources of this work. The other error source may be that for simplicity, the apex of the ice-cream cone is located in the center of the Sun, not at the solar surface as done by *Michalek and Gopalswamy* [2003]. In general, the method in this paper works well for the fast CMEs whose front edges are clear in the running different images. If the CME has relatively complex projected shape or the running different images are too faint, the result will be unstable.

[39] **Acknowledgments.** This work was supported by the Chinese Academy of Sciences under grant KZCX-SW-136, the National Natural Science Fund of China under grant 40336052 and 40474054, and the Innovation Fund of University of Science and Technology of China for the graduate students KD2004031. We wish to acknowledge the use of data from the SOHO/LASCO and SOHO/EIT observer and the data from "LASCO CME catalog." We also acknowledge the two referees for critical comments and suggestions to improve this work.

[40] Lou-Chuang Lee thanks G. Michalek and Xue-Pu Zhao for their assistance in evaluating this paper.

References

Brueckner, G. E., et al. (1995), The Large Angle Spectroscopic Coronagraph (LASCO), *Sol. Phys.*, *162*, 357.

Brueckner, G. E., J. P. Delaboudiniere, R. A. Howard, S. E. Paswaters, O. C. St. Cyr, R. Schwenn, P. L. Lamy, G. M. Simnett, B. Thompson, and D. Wang (1998), Geomagnetic storms caused by coronal mass ejections (CMEs): March 1996 through June 1997, *Geophys. Res. Lett.*, *25*, 3019.

Cane, H. V., and I. G. Richardson (2000), Interplanetary coronal mass ejections in the near-Earth solar wind during 1996–2002, *J. Geophys. Res.*, *108*(A1), 1156, doi:10.1029/2002JA009817.

Cane, H. V., I. G. Richardson, and O. C. St. Cyr (2000), Coronal mass ejections, interplanetary ejecta and geomagnetic storms, *Geophys. Res. Lett.*, *27*, 3591.

Delaboudiniere, J.-P., et al. (1995), EIT: Extreme-Ultraviolet Imaging Telescope for the SOHO mission, *Sol. Phys.*, *162*, 291.

Fisher, R. R., and R. H. Munro (1984), Coronal transient geometry. I- The flare-associated event of 1981 March 25, *Astrophys. J.*, *280*, 428.

Gopalswamy, N. (2002), Space weather study using combined coronagraphic and in situ observations, in *Space Weather Study Using Multipoint Techniques*, *COSPAR Colloq. Ser.*, edited by L.-H. Lyu, p. 39, Elsevier, New York.

Gopalswamy, N., A. Lara, R. P. Lepping, M. L. Kaiser, D. Berdichevsky, and O. C. St. Cyr (2000), Interplanetary acceleration of coronal mass ejections, *Geophys. Res. Lett.*, *27*, 145.

Gosling, J. T., D. J. McComas, J. L. Phillips, and S. J. Bame (1991), Geomagnetic activity associated with earth passage of interplanetary shock disturbances and coronal mass ejections, *J. Geophys. Res.*, *96*, 9831.

Harrison, R. A. (1986), Solar coronal mass ejections and flares, *Astron. Astrophys.*, *162*, 283.

Howard, R. A., D. J. Michels, N. R. Sheeley Jr., and M. J. Koomen (1982), The observation of a coronal transient directed at Earth, *Astrophys. J.*, *263*, L101.

Leblanc, Y., G. A. Dulk, A. Vourlidas, and J.-L. Bougeret (2001), Tracing shock waves from the corona to 1 AU: Type II radio emission and relationship with CMEs, *J. Geophys. Res.*, *106*, 25,301.

Liu, W., S. P. Plunkett, and X. P. Zhao (2002), A cone model for coronal mass ejections, in *Solar-Terrestrial Magnetic Activity and Space Environment*, *COSPAR Colloq. Ser.*, edited by H. Wang and R. Xu, p. 267, Elsevier, New York.

Michalek, G., and N. Gopalswamy (2003), A new method for estimating widths, velocities, and source location of halo coronal mass ejections, *Astrophys. J.*, *584*(1), 472.

Michalek, G., N. Gopalswamy, A. Lara, and P. K. Manoharan (2004), Arrival time of halo coronal mass ejections in the vicinity of the Earth, *Astron. Astrophys.*, *423*, 729.

Plunkett, S. P., B. J. Thompson, O. C. St. Cyr, and R. A. Howard (2001), Solar source regions of coronal mass ejections and their geomagnetic effects, *J. Atmos. Sol. Terr. Phys.*, *63*, 389.

Tsuneta, S., L. Acton, M. Bruner, J. Lemen, W. Brown, R. Caravalho, R. Catura, S. Freeland, B. Jurcevich, and J. Owens (1991), The soft X-ray telescope for the SOLAR-A mission, *Sol. Phys.*, *136*, 37.

Wang, Y. M., P. Z. Yee, S. Wang, G. P. Zhou, and J. X. Wang (2002), A statistical study on the geoeffectiveness of Earth-directed coronal mass ejections from March 1997 to December 2000, *J. Geophys. Res.*, *107*(A11), 1340, doi:10.1029/2002JA009244.

Wang, Y., C. L. Shen, S. Wang, and P. Z. Ye (2004), Deflection of coronal mass ejection in the interplanetary medium, *Sol. Phys.*, *222*, 329.

Webb, D. F., S. W. Kahler, P. S. McIntosh, and J. A. Klimchuck (1997), Large-scale structures and multiple neutral lines associated with coronal mass ejetcions, *J. Geophys. Res.*, *102*, 24,161.

Webb, D. F., E. W. Cliver, N. U. Crooker, O. C. St. Cyr, and B. J. Thompson (2000), Relationship of halo coronal mass ejections, magnetic clouds, and magnetic storms, *J. Geophys. Res.*, *105*, 7491.

Xie, H., L. Ofman, and G. Lawrence (2004), Cone model for halo CMEs: Application to space weather forecasting, *J. Geophys. Res.*, *109*, A03109, doi:10.1029/2003JA010226.

Yashiro, S., N. Gopalswamy, G. Michalek, O. C. St. Cyr, S. P. Plunkett, N. B. Rich, and R. A. Howard (2004), A catalog of white light coronal mass ejections observed by the SOHO spacecraft, *J. Geophys. Res.*, *109*, A07105, doi:10.1029/2003JA010282.

Zhao, X. P., S. P. Plunkett, and W. Liu (2002), Determination of geometrical and kinematical properties of halo coronal mass ejections using the cone model, *J. Geophys. Res.*, *107*(A8), 1223, doi:10.1029/2001JA009143.

X. K. Dou, C. B. Wang, and X. H. Xue, School of Earth and Space Sciences, University of Science and Technology of China, Hefei, Anhui, 230026, China. (dou@ustc.edu.cn; cbwang@ustc.edu.cn; xuexh@mail.ustc.edu.cn)